

A comparison of four direct geometry time-of-flight spectrometers at the Spallation Neutron Source

M. B. Stone, J. L. Niedziela, D. L. Abernathy, L. DeBeer-Schmitt, G. Ehlers, O. Garlea, G. E. Granroth, M. Graves-Brook, A. I. Kolesnikov, A. Podlesnyak, and B. Winn

Citation: *Review of Scientific Instruments* **85**, 045113 (2014); doi: 10.1063/1.4870050

View online: <http://dx.doi.org/10.1063/1.4870050>

View Table of Contents: <http://scitation.aip.org/content/aip/journal/rsi/85/4?ver=pdfcov>

Published by the [AIP Publishing](#)

Articles you may be interested in

[A time-of-flight backscattering spectrometer at the Spallation Neutron Source, BASIS](#)

Rev. Sci. Instrum. **82**, 085109 (2011); 10.1063/1.3626214

[Comparison between time-of-flight spectra measured at a spallation source and at a high flux reactor](#)

Rev. Sci. Instrum. **59**, 370 (1988); 10.1063/1.1140207

[Fast Neutron Time-of-Flight Spectrometer](#)

Rev. Sci. Instrum. **33**, 1231 (1962); 10.1063/1.1717735

[Fast Neutron Time-of-Flight Spectrometer](#)

Rev. Sci. Instrum. **30**, 963 (1959); 10.1063/1.1716441

[Medium-Energy Neutron Time-of-Flight Spectrometer](#)

Rev. Sci. Instrum. **28**, 245 (1957); 10.1063/1.1715850

The new SR865 *2 MHz Lock-In Amplifier ... \$7950*



SR865 2 MHz Lock-In Amplifier

Features

- Intuitive front-panel operation
- Touchscreen data display
- Save data & screen shots to USB flash drive
- Embedded web server and iOS app
- Synch multiple SR865s via 10 MHz timebase I/O
- View results on a TV or monitor (HDMI output)

Specs

- 1 mHz to 2 MHz
- 2.5 nV/√Hz input noise
- 1 μs to 30 ks time constants
- 1.25 MHz data streaming rate
- Sine out with DC offset
- GPIB, RS-232, Ethernet & USB

SRS Stanford Research Systems
www.thinkSRS.com · Tel: (408)744-9040

A comparison of four direct geometry time-of-flight spectrometers at the Spallation Neutron Source

M. B. Stone,¹ J. L. Niedziela,² D. L. Abernathy,¹ L. DeBeer-Schmitt,² G. Ehlers,¹ O. Garlea,¹ G. E. Granroth,³ M. Graves-Brook,² A. I. Kolesnikov,⁴ A. Podlesnyak,¹ and B. Winn¹

¹*Quantum Condensed Matter Science Division, Oak Ridge National Laboratory, Oak Ridge, Tennessee 37831, USA*

²*Instrument and Source Division, Oak Ridge National Laboratory, Oak Ridge, Tennessee 37831, USA*

³*Neutron Data Analysis and Visualization Division, Oak Ridge National Laboratory, Oak Ridge, Tennessee 37831, USA*

⁴*Chemical and Engineering Materials Division, Oak Ridge National Laboratory, Oak Ridge, Tennessee 37831, USA*

(Received 21 January 2014; accepted 17 March 2014; published online 16 April 2014)

The Spallation Neutron Source at Oak Ridge National Laboratory now hosts four direct geometry time-of-flight chopper spectrometers. These instruments cover a range of wave-vector and energy transfer space with varying degrees of neutron flux and resolution. The regions of reciprocal and energy space available to measure at these instruments are not exclusive and overlap significantly. We present a direct comparison of the capabilities of this instrumentation, conducted by data mining the instrument usage histories, and specific scanning regimes. In addition, one of the common science missions for these instruments is the study of magnetic excitations in condensed matter systems. We have measured the powder averaged spin wave spectra in one particular sample using each of these instruments, and use these data in our comparisons. © 2014 AIP Publishing LLC. [<http://dx.doi.org/10.1063/1.4870050>]

I. INTRODUCTION

For nearly 70 years, neutron spectroscopy has been applied to study materials in the fields of condensed matter physics, biology, chemical sciences, geology, and mineralogy.¹ The broad applicability and importance of neutron scattering is recognized in the 1994 Nobel Prize awarded to Shull and Brockhouse for the development of neutron diffraction and spectroscopy techniques. The mass of the neutron and the distribution of neutron wavelengths available from spallation- and reactor-based neutron sources have made inelastic neutron spectroscopy an especially useful probe to study excitations in the sub-millielectron volt to the electron volt energy range. This covers a broad range of physical phenomena, including lattice excitations, molecular spectroscopy, magnetic excitations, and crystal-field excitations. There are several types of instruments which exploit the velocity distribution of thermalized neutrons, and the neutron's magnetic moment in order to accurately measure these excitations.²⁻⁵

The direct geometry chopper spectrometer (DGCS) is a type of inelastic neutron scattering instrument in use at both spallation- and reactor-based neutron sources.^{5,6} A DGCS instrument uses a series of rotating absorbers to monochromate the spectrum of neutrons being emitted from the neutron source, thus providing a beam of neutrons with a well defined energy and momentum. These monochromatic neutrons are then scattered from a sample, and the final neutron energy and momentum are found from the final neutron velocity and scattering angle using time-of-flight techniques and conservation principles. DGCS instruments have become prevalent at spallation neutron sources due to the pulsed nature of the neutron

beams.⁷⁻¹⁸ Typically there are multiple DGCS instruments at spallation sources in order to exploit the differences in spectra emitted from different neutron moderators, and a suite of such instrumentation will cover a range of energy and wave-vector transfers with varying degrees of resolution and neutron flux.

Presently there are four DGCS instruments at the Spallation Neutron Source (SNS) at the Oak Ridge National Laboratory. These are the cold neutron chopper spectrometer (CNCS), the hybrid spectrometer (HYSPEC), the fine-resolution Fermi chopper spectrometer (SEQUOIA), and the wide angular-range chopper spectrometer (ARCS). While there are individual instrumentation manuscripts published for these instruments,¹⁹⁻²¹ we examine here how these instruments compare directly to one another in terms of flux and resolution, and show that each instrument fits the niche for which it was designed.²²⁻²⁴ These instruments have been used to examine a broad range of phenomena.²⁵ In this report, we compare these instruments in a region of phase space where their capabilities overlap by examining the measured scattering from CrCl₂, an $S = 2$ antiferromagnet.

II. INSTRUMENTS

Early design characterizations²²⁻²⁴ provided general guidance for how the DGCS instruments at the SNS should be built. Though there are quantitative differences between the expected and measured performance, the present study shows that each instrument is optimized for the energy and wave-vector, Q , range for which it was designed.

The SNS produces neutrons by colliding a beam of high energy protons with a liquid mercury target. The proton beam

TABLE I. Instrument parameters for the DGCS suite at the SNS. The source-beam monitor distance listed here corresponds to the beam monitor used for characterizing the instruments throughout the manuscript. This beam monitor is located after the last monochromating element of the DGCS. The source-downstream beam monitor distance corresponds to the beam monitor after the sample position, and this kind of monitor is present only at ARCS and SEQUOIA. Values listed are as of August 2013. c-IH corresponds to the coupled liquid hydrogen moderator and apd-H₂O corresponds to the ambient, poisoned, decoupled water moderator. The width and height of the beam noted here corresponds to the design value, which does not account for beam divergence. Also, all four instruments have the ability to tailor the final size of the beam by the use of boron carbide slits positioned upstream of the sample.

Parameter	CNCS	HYSPEC	SEQUOIA	ARCS
Moderator	c-IH	c-IH	apd-H ₂ O	apd-H ₂ O
Source-beam monitor distance (m)	34.85	37.38	18.23	11.831
Source-downstream monitor distance (m)	n/a	n/a	29.003	18.5
Source-sample distance (m)	36.26	40.77	20.01	13.6
Height of beam at sample (cm)	5	3.5	5	5
Width of beam at sample (cm)	1.5	3.5	5	5
Detector tube diameter (cm)	2.54	2.54	2.54	2.54
Detector tube length (m)	2	1.2	1.2	1
Mean sample-detector distance (m)	3.54	4.54	5.53	3.21
Minimum equatorial scattering angle (deg.)	3.8	0 ^a	2.0	2.4
Maximum equatorial scattering angle (deg.)	135	135	59.3	136.0
Maximum out of plane scattering angle (deg.)	16	7.5	19.4	27
Solid angle detector coverage ^b (Sr.)	1.606	0.226	0.863	2.196
Incident energy range (meV) ^c	1–80	4–60	8–2000	15–1500
Range of energy resolution (% <i>E</i>) ^d	1–5	3–5	1–3	3–5
Radial collimator	Yes	Yes	No	Yes
Entry into user program	2009	2013	2010	2008
Reference	19		20, 34	21

^aThe HYSPEC detector array is 60° wide in the equatorial scattering direction and can operate even at 0° scattering angle. In practice accurate measurements can only be made down to between 2° and 4° in scattering angle.

^bThe solid angle detector coverage was determined by summing up the solid angle of all detector pixels using the Mantid software.³¹

^cIncident energies outside of the range listed are available with reduced flux.

^dEnergy resolutions are quoted as a full width at half maximum of the elastic scattering peak in units of a percentage of the incident energy. Coarser energy resolution is also available at these instruments.

is created by extracting a 1 ms pulse of H[−] ions from a plasma ion source, using an electrostatic “chopper” to split the 1 ms pulse into a train of 1 μs pulses, which are accelerated to high energy using a 335 m long linear accelerator. The H[−] ions are then stripped of their electrons creating a beam of bare proton pulses. These pulses are then directed into an accumulator ring where they are stacked into a single pulse approximately 700 ns wide, and the collected pulse is then extracted from the accumulator ring and directed to the target. The high energy protons produce neutrons either by direct spallation reactions where neutrons are ejected from the mercury nucleus as a result of the collision, or by the proton directly exciting the mercury nucleus to the point where the mercury nuclei de-excite through evaporation of neutrons.²⁶ The SNS design specification is 1.4 MW, 60 Hz operation, with a 1 GeV proton beam. The nominal source operation as of 2013 is between 850 kW and 1.2 MW, 60 Hz operation with an ~0.9 GeV proton beam.²⁷

The neutron spectrum produced during the proton-target collision can contain neutrons up to the energy of the incident proton beam, so the SNS employs a system of neutron moderators to reduce the neutron energies into a range useful for the energy scales of scientific interest at the facility. There are three moderator types: a coupled liquid hydrogen moderator (c-IH), an ambient, poisoned, decoupled water moderator

(apd-H₂O), and a supercritical decoupled poisoned liquid hydrogen moderator (sdp-IH). The expected performance of the moderators was modeled²⁸ and the various instrument papers confirm their expected performance.^{19–21} The corresponding neutron moderators for the DGCS instruments are listed in Table I.

The DGCS instruments at the SNS are constructed with similar elements, including neutron super mirror guides, control systems, detector type, and neutron choppers. Neutron guides were supplied by commercial vendors and aid in the transport of neutrons to the sample position. As neutrons travel down the beam path, they reflect off the neutron mirror surfaces, increasing the total number of neutrons transported to the sample position. The reflectivity of the coating is dependent on the neutron wavelength, so the guide is also able to assist in energy selection of the primary neutron beam. Specially constructed guide pieces may also offer flexibility in resolution and beam focussing. Chopper elements are similar between beamlines, with interchangeability between beamlines available; for example, ARCS and SEQUOIA use a common design of Fermi chopper rotor and motor, allowing different slit packages to be inserted into the rotor to provide optimized resolution and flux conditions for each instrument or for particular experiments. Information about the chopper timing is integrated into the neutron data stream

to allow for later filtering of pulses. The control systems at the instruments are similar, with satellite computers controlling ancillary equipment (e.g., choppers, sample environment, motors, etc.), while the fast neutron acquisition is done by electronics developed at the facility, and tied to the primary accelerator timing system. For detectors, all four instruments employ ^3He linear position sensitive tube detectors (LPSDs) that are assembled into 8-packs. The full width at half maximum (FWHM) spatial resolution along these tubes is approximately 1% of their length.²⁹ In all DGCS cases, the 8-packs are arrayed in a cylindrical geometry around the sample position with the axis of the cylinder oriented vertically. The 8-packs consist of stainless steel cylindrical detector tubes with diameters and lengths as listed in Table I. Using these 8-packs, each neutron event is recorded and timed with a 100 ns clock from a set offset to when the injection signal is sent to the kicker magnet of the accelerator. Data are streamed from the detector electronics, and each detected neutron is stored as a unique “event” with the information about the pixel where the neutron was detected, the time stamp of detection, and from which pulse of the accelerator the detected neutron originated.²⁹ Collecting the data in this “event-data” mode allows maximal retention of information, and later correlation with external parameters, such as a pulsed magnetic field,³⁰ sample temperature, or sample rotation angle.³² Summaries of the beamline configurations are given in Table I.

Details of the detector configurations for the individual DGCS instruments are shown in Figs. 1 and 2. Here we can see the large forward detector coverage of the SEQUOIA instrument as well as the large consistent coverage up to large scattering angles for the CNCS and ARCS instruments. HYSPEC has smaller coverage but is able to move the detector bank over the full range of scattering angles up to approximately 135° , or in a position such that it straddles the incident beam. The modular 8-pack detector design provides flexibility in detector installation, however it also yields gaps in detector coverage. This can be seen in the double peak structure for the ARCS histogram of detector positions shown

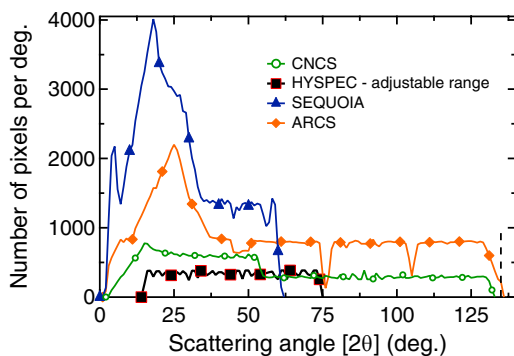


FIG. 1. Number of detector pixels as a function of the scattering angle 2θ for the four DGCS instruments at the SNS. The pixel number has been histogrammed in one degree bins. HYSPEC is able to adjust the location of its detector range. The upper limit to HYSPEC’s detector coverage is indicated with a vertical dashed line at approximately 135° ; because it can continuously move its detector through the incident beam, there is no lower limit of HYSPEC’s detector coverage. Markers are plotted at 10° intervals for presentation.

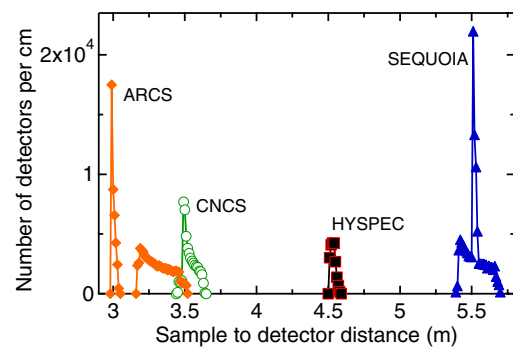


FIG. 2. Number of detector pixels as a function of distance from the sample position to the detector position for the four DGCS instruments at the SNS. The pixel number has been histogrammed to 1 cm increments.

in Fig. 2. We also note that the CNCS and SEQUOIA instruments currently have room available for additional detectors.

A. CNCS

CNCS is a high-resolution, cold neutron chopper spectrometer located on the coupled cryogenic H_2 (c-1H) moderator. Typical incident energy selections range between 1 and 50 meV with a typical energy resolution of between 2% and 3% of the incident energy at the elastic line. The sample and sample environment are positioned in air. The typical sample environment in use at CNCS is a pumped liquid helium cryostat. To reduce air scattering, the CNCS detectors are housed in an argon environment with a 0.5 mm thick aluminum window between the sample area and the detector tank. The window is radially centered a distance of 0.76 m from the sample location. No impact of the argon atmosphere on the scattering measurements has been observed. However, it has been found to be very important to place a beam stop after the sample position and as close to the sample as possible to reduce the background from the direct beam incident upon the aluminum window. The detector array consists of 50 ^3He LPSD 8-packs positioned 3.5 m from the sample position. For energy selection, the CNCS employs four chopper assemblies: two frame overlap choppers, a Fermi chopper with a translation stage to switch between slit packages optimized for transmission >25 and <25 meV neutrons, and a high-speed double disk chopper used to switch between high-resolution, high-flux, and an intermediate mode of operation. Additionally, a curved supermirror guide is used to transport the beam from the moderator to the sample position. A set of boron carbide slits downstream of the final chopper can tailor the beam to the sample size.

B. HYSPEC

HYSPEC is a high-intensity, medium-resolution, cold to thermal DGCS optimized for measurement of excitations in small single-crystal specimens. HYSPEC employs a hybrid design by adding to a traditional time-of-flight spectrometer the pre-sample Bragg optics found on a triple-axis spectrometer. The Bragg optics allow the use of vertical focusing prior to the sample position to increase the flux on sample. In addition,

the Bragg optics allow for the use of a Heusler monochromator for neutron polarization techniques. HYSPEC is located on a different c-1H moderator than CNCS. The incident neutron beam is first monochromated using a Fermi chopper. The Fermi chopper, at 37.17 m from the moderator, has straight blades 10 mm long with 0.6 mm slits, and allows a tradeoff between flux and resolution by changing rotation frequency between 30 Hz and 420 Hz, but is usually operated between 180 Hz and 420 Hz. A narrow bandwidth vertical rotation axis T_0 chopper at 8.5 m blocks the highest energy neutrons generated when the proton pulse hits the target. Two disc choppers, T1A and T1B, at 9.4 m and 36.46 m, respectively, reject frame overlap neutrons and neutrons that would have been transmitted by the Fermi chopper running at frequencies other than 60 Hz.

After the choppers set the incident energy, Bragg optics, located 1.4–1.8 m from the sample position, vertically focus the neutron beam from a 40 mm wide, 150 mm tall guide onto the sample. At an incident energy of 15 meV and 1.8 m from the sample, the profile of the beam at sample position is roughly $35 \times 35 \text{ mm}^2$. The beam profile may be further defined using motorized slits. Horizontal divergence of the beam may be further defined using 20 or 40 minute Soller collimators, but these are rarely used. When operating in unpolarized mode, the Bragg focusing optics used are pyrolytic graphite with 1.2° FWHM mosaic. The typical sample environment in use at HYSPEC is a pumped liquid helium cryostat.

Neutrons are detected in a set of 20 LPSD 8-packs located 4.5 m from the sample position. The detector bank covers an angle range of 60° in the horizontal scattering plane, but can be rotated about the sample, providing measurement at scattering angles of up to $\pm 135^\circ$ depending on incident energy. The HYSPEC detector bank can also be positioned so that the detector bank straddles the incident neutron beam downstream of the sample; in this manner, small Q excitations can be measured for both positive and negative scattering angles. The HYSPEC detector assembly contains a vessel that provides an argon atmosphere path between 0.8 and 4.4 m after the sample position, with aluminum windows defining the volume. The 8-pack detectors are located in air just outside the argon vessel, making the detectors and detector electronics easily accessible.

Full and partial neutron polarization analysis will soon be deployed on HYSPEC,³³ and will be accomplished by using a Heusler crystal array to polarize the incident beam, and either a ^3He spin filter or super-mirror wide-angle polarization analyzers for the scattered beam. Both CNCS and HYSPEC employ tail-mounted sample environments in air, which is a configuration common to triple axis spectrometers, and which provides some additional flexibility in configuration.

C. SEQUOIA

SEQUOIA is a fine resolution, direct geometry, thermal to epithermal Fermi chopper spectrometer. The neutron beam originates from the apd- H_2O moderator. A Fermi chopper, located 18 m downstream of the moderator and 2 m upstream of the sample, monochromates the beam. Multiple Fermi chop-

pers are available for use of which two can be placed on a motorized translation table for quick changes during an experiment. The default choices are the 100 meV Fermi chopper with 2.03 mm slits and a channel curvature of 0.58 m, and the 700 meV Fermi chopper, with 3.6 mm slits and a channel curvature of 1.53 m (the so-called *sloppy chopper*). The energy associated with a chopper, i.e., 700 meV Fermi chopper, corresponds to the energy of maximum transmission for the maximum Fermi chopper speed of 600 Hz. Additional Fermi choppers are available. Specifically one with 1.5 mm spacing and 1.83 m curvature for fine resolution at high energies, and another with 0.5 mm spacing and 1.53 m curvature, for the cases where much of the flux can be sacrificed for fine resolution. This latter chopper is routinely shared with ARCS. A vertical rotation axis T_0 chopper is located 9.8 m from the moderator. Its primary purpose is to block the highest energy neutrons generated when the proton pulse hits the target, and also serves as a bandwidth limiting chopper to control when neutrons are available to the Fermi chopper. Neutron guide is utilized to provide a high flux of neutrons on a sample that can be as large as 50 mm by 50 mm. The LPSDs are assembled into a cylindrical detector array consisting of $\sim 110\,000$, 12 mm tall by 25.4 mm wide pixels with a radius of 5.5 m around the sample position. The detectors are housed in a cryogenic vacuum environment. The typical sample environment at SEQUOIA is a closed cycle ^4He refrigerator. One of the science missions shared between SEQUOIA and CNCS is the study of magnetic materials. The magnetic form factor for scattering neutrons decreases quickly with increasing wave-vector transfer. The larger incident energies available at the SEQUOIA spectrometer allow for measurement of a substantial portion of the magnetic form factor with a smaller angular range, whereas CNCS operates at much lower incident energies and therefore must have detectors available to larger scattering angles to measure a large portion of the wave-vector dependent magnetic form factor.

D. ARCS

ARCS is a high-flux, direct geometry thermal chopper spectrometer. The neutron beam originates from the same decoupled ambient temperature H_2O moderator as SEQUOIA. The ARCS instrument has 115 LPSD 8-pack modules located 3.0–3.5 m from the sample position in an angular range from -28° to 135° in the scattering plane. To reduce scattering from the atmosphere, the ARCS detectors are housed in a cryogenic vacuum environment. A vertical axis T_0 chopper is located 8.77 m from the moderator. A Fermi chopper translation table is located 11.61 m from the moderator and 2 m upstream of the sample, and typically installed options include a chopper with slit packages optimized for 100 meV, 700 meV, and an open position to allow unchopped (“white”) beam measurements. Both of the 700 and 100 meV slit packages consist of 1.9 mm slits and a channel curvature of 1.5 m and 0.55 m for the 700 and 100 meV chopper, respectively. The nominal beam size is 50 mm \times 50 mm, but a set of motorized slits constructed of boron carbide are located ≈ 0.25 m from the sample position allowing fine tailoring of the beam size. The typical sample environment at ARCS is a closed

cycle ^4He refrigerator. Both the ARCS and SEQUOIA instruments make use of a large gate valve between a sample vacuum chamber and a detector vacuum chamber. This allows one to vent the sample chamber for sample changes without venting the very large detector chamber and eliminates additional windows in the scattered neutron flight path. The ARCS and SEQUOIA instruments were designed to be complementary in terms of the neutron flux and resolution available for the same range of incident energies.²²

III. COMPARISON OF PRIMARY SPECTROMETERS

All four of the DGCS instruments are equipped with a low-efficiency beam monitor upstream of the sample position. The individual locations of this beam monitor relative to the sample and moderator are noted in Table I. The monitor counts are histogrammed as a function of time-of-flight for every measurement at these instruments. We have *data-mined* prior acquired data from these instruments to determine the intensity and energy resolution as a function of the incident energy used at the individual beamlines. We also use these data to examine the distribution of incident energies being used at these instruments.

For the SEQUOIA and ARCS instruments, we determine the incident energy based upon numerical fitting of peaks in the beam monitor data. These instruments have a second beam monitor located in the beam-stop downstream of the sample position. By knowing the relative distance between the two beam monitors and the time-of-flight for the neutrons traversing this distance, one can determine the velocity and therefore the incident energy, E_i , of the monochromatic neutrons. In addition to E_i , this procedure also determines the time relative to the instrument timing signal that the neutrons are emitted from the moderator. This time is referred to as the emission time, t_0 . Figure 3 shows the emission time as a function of the incident energy for the ARCS and SEQUOIA instruments. As the incident energy increases, the time it takes the neutrons to be emitted from the moderator decreases, which reflects a

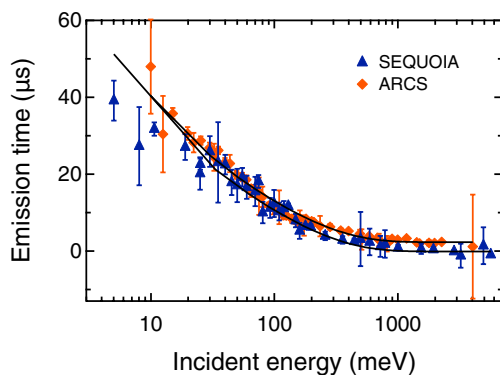


FIG. 3. Emission time, t_0 , as a function of incident energy for the SEQUOIA and ARCS instruments. Values were determined using the Gauss-Ikeda-Carpenter method of fitting beam monitor data as described in the text. The beam monitor data were collected over the working lifetimes of these instruments until approximately May 2013. The solid lines are a simultaneous fit to the sum of a power law and exponential function as described in the text. The error bars correspond to the standard deviation in the mean histogrammed value of the emission time.

shorter moderation time. We parameterize these data with a function that decays to a constant for large incident energies and diverges as one approaches zero incident energy. The sum of a constant, a power law, and an exponential represents these data well:

$$t_0 = A + |B|E_i^p + |C| \exp\left(-\frac{E_i}{\tau}\right). \quad (1)$$

We simultaneously fit the ARCS and SEQUOIA data to Eq. (1) using common values of B , p , C , and τ and allowing the A values to vary for the two instruments. The solid lines in Fig. 3 are the result of this fit and provide a reasonable representation of the data. The difference in the fitted A values is only $2.4(2) \mu\text{s}$, indicating that the timing distribution system only introduces a small offset for the two instruments. The fitted parameters were $B = 0.02$, $p = -0.41$, $C = 4400$, and $\tau = 280$.

For the ARCS and SEQUOIA instruments, the intensity as a function of time-of-flight, $I(t)$, for the second beam monitor is well-represented by a modified Ikeda-Carpenter function:

$$I(t) = B + A \frac{\alpha}{\Gamma(\nu + 1)} \left(\alpha \left(t_p + \frac{\nu}{\alpha} - t \right) \right)^\nu \times \exp\left(-\alpha \left(t_p + \frac{\nu}{\alpha} - t \right)\right), \quad (2)$$

where B is a background term, A is a multiplicative scaling factor, Γ is the gamma function, t_p is the peak position, and α and ν are fitting parameters controlling the peak shape.³⁵ The intensity from the second term is zero for $t > t_p + \frac{\nu}{\alpha}$. The short distance between the Fermi chopper and the first beam monitor allows one to use a Gaussian approximation to describe the peak in the time-of-flight spectrum of this beam monitor. Figure 4 shows beam monitor data for both the SEQUOIA and ARCS instruments for 100 meV incident energy neutrons. The distance from the moderator to SEQUOIA's

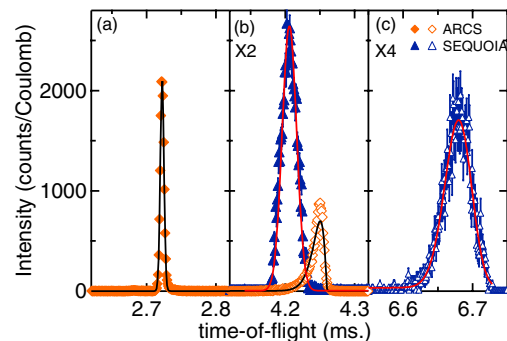


FIG. 4. Histogrammed beam monitor scattering intensity as a function of time-of-flight. Data are from the ARCS and SEQUOIA instruments using 100 meV neutrons. All three panels are the same width in milliseconds. Panel (b) is plotted on one half the intensity scale of panel (a). Panel (c) is plotted on one fourth the intensity scale of panel (a). Solid symbols correspond to data from the first beam monitor (located after the Fermi chopper and before the sample). Open symbols correspond to data from the second beam monitor (located after the sample). The solid lines through the beam monitor two data correspond to fits to an Ikeda-Carpenter function as described in Eq. (2). The solid lines through the beam monitor one data correspond to simple Gaussian fits. The histogrammed beam monitor data have been normalized per Coulomb of charge on the spallation target.

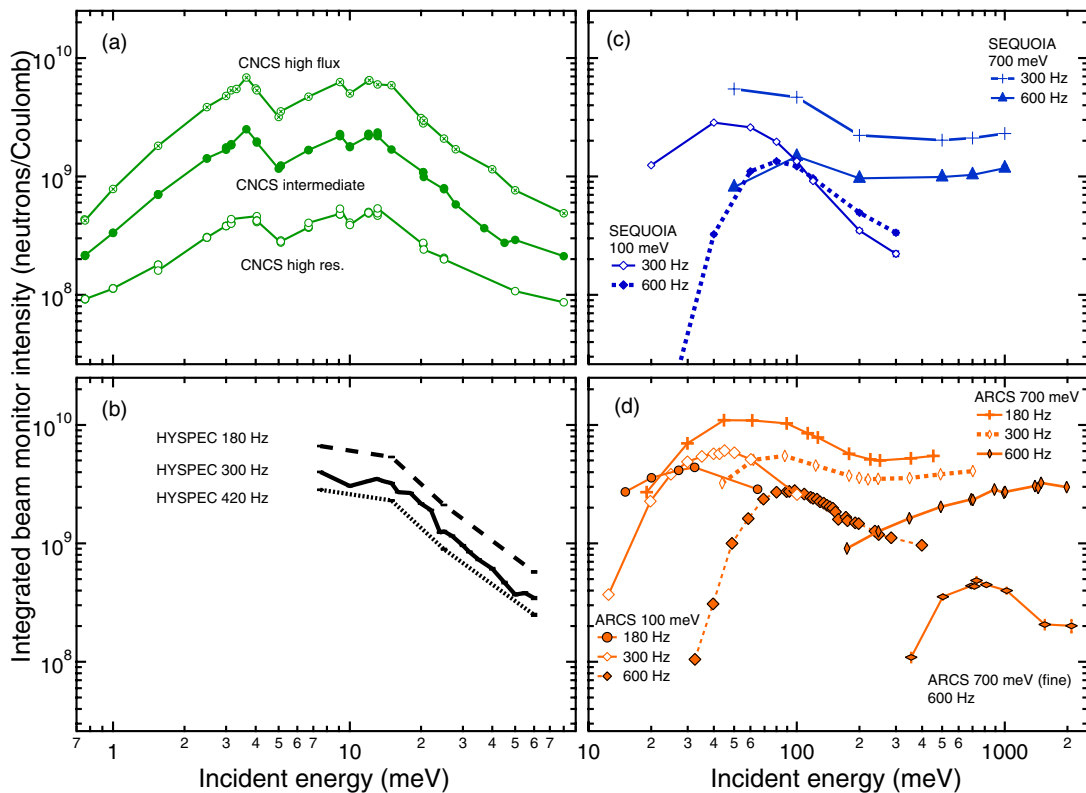


FIG. 5. Relative beam monitor integrated intensity as a function of incident energy for the (a) CNCS, (b) HYSPEC, (c) SEQUOIA, and (d) ARCS instruments at the SNS. The curves are colored according to the corresponding instrument being used. The vertical axis is in units of neutrons per Coulomb of charge on the SNS target. For 1.05 MW operation, charge accumulates at a rate of approximately 4 C/h. The particular operations of the instrument or Fermi chopper employed are noted in the figure. These data correspond to integrating the beam monitor intensity for the beam monitor located immediately prior to the sample at the respective DGCS. All of the beam monitor spectra were collected in $1 \mu\text{s}$ histograms. This integrated intensity has been normalized to the amount of proton charge collected on the spallation target. A wavelength dependent efficiency correction has also been applied to this integrated intensity. Differences in beam size, beam monitor size, or details of how the beam monitor is shielded differently at each instrument were not accounted for in the normalization.

first beam monitor (18.23 m) is very close to the distance from the moderator to ARCS's second beam monitor (18.5 m) as shown in Fig. 4(b). The beam monitor spectra agree well with the Gaussian lineshape and modified Ikeda-Carpenter function used for the first and second beam monitor, respectively.

The CNCS and HYSPEC instruments do not have a beam monitor located behind the sample position. Therefore, a similar analysis to determine the moderator parameters is not possible. For these instruments, the incident energy is determined using the time-of-flight for the elastic scattered neutrons and the peak time-of-flight position in the beam monitor located before the sample.

To compare the neutron flux and energy resolution of the four DGCS instruments we use the histogrammed time-of-flight data from the beam monitor before the sample. We numerically calculate the area under the monochromatic peak by integrating the histogrammed intensity as a function of time-of-flight. A time-of-flight value based on the requested incident energy is used to calculate a time range around the primary beam peak where there should be no counts for a given instrument configuration. This range is then used to determine a linear background in the vicinity of the peak, and this background is subtracted from the scattering intensity prior to integration. We also correct the integrated intensity based upon the known wavelength dependent efficiency of the beam monitors. This integrated intensity serves as a measure of the

instrumental neutron flux that can be directly compared between the four instruments. Figure 5 and the figures in the supplementary material show the determined integrated intensity as a function of incident energy for the DGCS instrument suite at the SNS.³⁶

We also fit the beam monitor data to a Gaussian peak with a background determined as described above. The FWHM in microseconds of this peak is then used as a measure of one component of the incident beam energy resolution. We convert this value to be a FWHM in energy using

$$\delta E = \frac{2E_i}{t} \delta t, \quad (3)$$

where δE is the FWHM in incident energy at the beam monitor, t is the peak in the time-of-flight spectrum, and δt is the FWHM of the time-of-flight spectrum measured by the beam monitor for the monochromatic peak. This is a measure of the energy distribution of the neutron beam at the beam monitor position immediately prior to the sample position. This energy distribution, when combined with the chopper opening time, the moderator neutron emission time uncertainty, sample mosaic and shape, and the details of the secondary spectrometer, controls the energy and Q resolution of the instrument.^{5,20,21} Figure 6 shows this component of the energy distribution as a function of incident energy for the DGCS instruments. Since this part is the most readily variable contribution to the energy

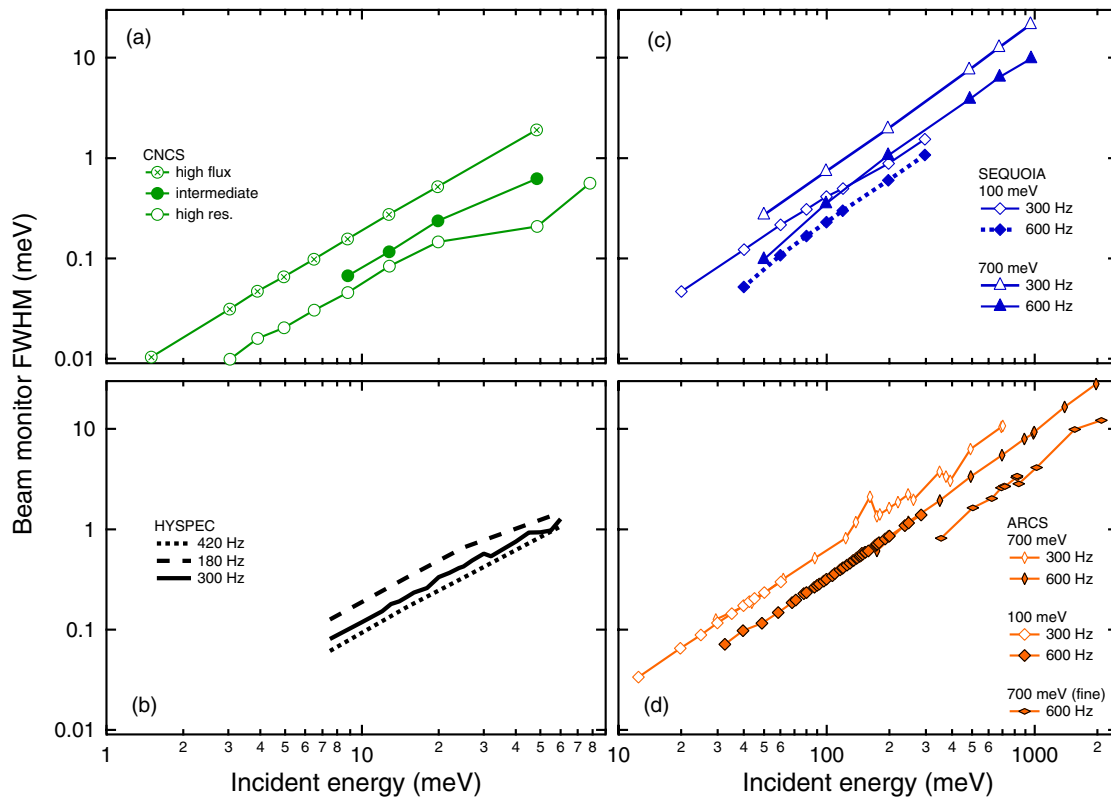


FIG. 6. Full width at half maximum (FWHM) of the incident energy distribution as a function of incident energy for the (a) CNCS, (b) HYSPEC, (c) SEQUOIA, and (d) ARCS instruments at the SNS. The value plotted is the FWHM contribution to the incident energy distribution as measured at the beam monitor closest to the sample position. This value is further described in the text.

resolution, Fig. 6 and figures in the supplementary material³⁶ illustrate how each instrument can be tailored to the energy resolution needs of a specific experiment.

From Figs. 5 and 6 one can see the different regimes that these instruments work within: using cold or thermal neutrons, or choosing higher flux at the expense of energy resolution. The ARCS and SEQUOIA instruments are able to tailor their flux and energy resolution through the particular Fermi chopper slit package and rotation frequency being employed. ARCS typically has more neutron flux available than SEQUOIA; however, SEQUOIA typically has improved energy resolution for the most often used slit packages. Both the ARCS 100 and 700 meV Fermi chopper were made with the same slit spacing but a different radius of curvature. For a given chopper frequency, this results in the same power law curve for the FWHM energy resolution contribution as a function of incident energy. For ARCS a highly collimated (0.51 mm slit size) Fermi chopper was also prepared and used for measuring high energy excitations in quantum liquids. This chopper improved the energy resolution but reduced the neutron flux by a factor of 5.4. CNCS and HYSPEC are also complementary instruments. CNCS is able to provide improved energy resolution over HYSPEC for certain modes of operation. The neutron flux at HYSPEC is also greater than that at CNCS for certain modes of operation. In their coarsest energy resolution configurations, both instruments perform in a very similar manner. The local minimum in flux at approximately 5 meV for CNCS is believed to be due to Bragg scattering at the aluminum windows at the boundaries of the evac-

uated guide sections of the primary spectrometer. We note that the wave-vector resolution of the instrumentation is not accounted for in this comparison.

We have also examined the chosen incident energies for each DGCS while in the user program at the SNS. While Figs. 5 and 6 demonstrate the capabilities of the instrumentation, the data shown in Fig. 7 indicate how the instruments are actually being used. We histogrammed all of the incident energies used at the DGCS instruments into logarithmically spaced energy bins. The data files were weighted by the amount of proton charge accumulated on the spallation target, not by the total measurement time. The instruments which use the same moderator share a similar distribution in incident energies. We also note that there is significant overlap in incident energies used for the four instruments between 10 and 60 meV. Interestingly, there are some incident energies which have become favorites of the user community. The histograms in Fig. 7 clearly show that the instruments are operated within their designed energy range.²³ Furthermore, it clearly identifies other operational parameters of the instruments. First, the dips in usage for CNCS at energies near 29.6, 7.5, and 3.3 meV and for HYSPEC at energies of ≈ 10 and ≈ 30 meV are due to transitioning between accelerator frames, which results in contamination of the desired measurement interval by prompt neutrons from the next accelerator pulse. Similarly, the dip in the low usage in the histogram for SEQUOIA around $E_i = 12$ meV arises from boundary of the first and second frames which occurs at $E_i = 12.2$ meV.

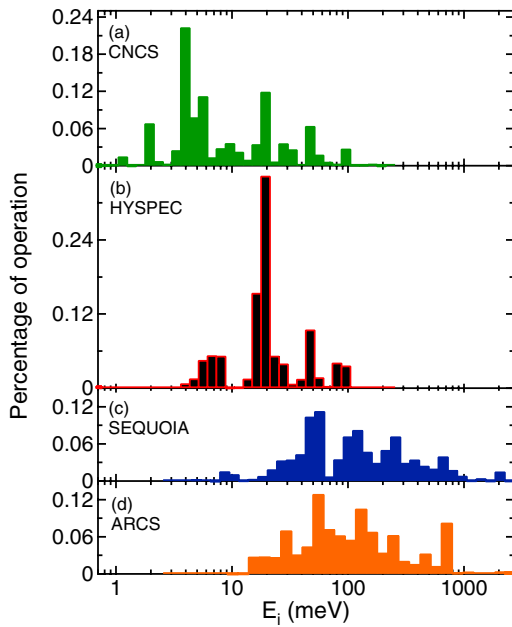


FIG. 7. Histogram of the percent of total coulombs of charge on the spallation target versus the incident energy at which the measurements were performed for the CNCS, HYSPEC, SEQUOIA, and ARCS DGCS. The vertical axis scaling is identical for the four panels.

We have made a phase space diagram of the available energy- and wave-vector transfer coverage of the four DGCS instruments based upon how they are being used. Figure 8 shows the range of wave-vector transfers available for different values of incident energy. The value of incident energy was limited to the middle 90% of energies used at the instruments as shown in Fig. 7. This eliminates some of the measurements where users may have operated beyond instruments' capabilities. This figure further illustrates the

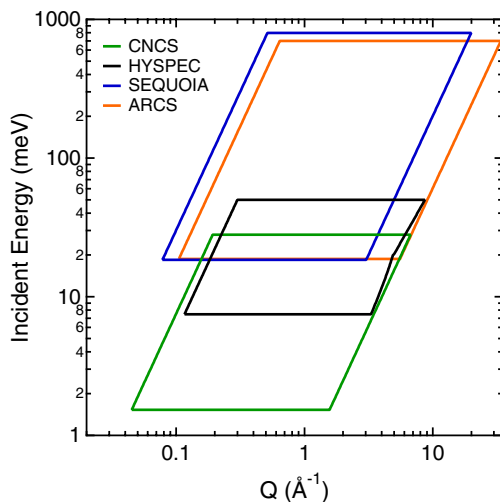


FIG. 8. Ranges of incident energy used in 90% of the measurements to date at CNCS, HYSPEC, SEQUOIA, and ARCS. The corresponding range of wave-vector transfer for the elastic scattering is plotted on the x-axis. The far left and right boundaries are defined by the minimum and maximum scattering angles that can be measured for the corresponding instrument. A 3.5° value was used for the HYSPEC minimum angle. All the other instruments use their absolute minimum angle from Fig. 1.

complementary nature of the instrumentation and suggests ranges of phase space which additional instrumentation may appropriately cover.

IV. COMPARISON OF CrCl_2 MEASUREMENTS

CrCl_2 is a well-characterized $S = 2$ quasi-one-dimensional antiferromagnet with a large on-site anisotropy.³⁷⁻⁴¹ The magnetic excitations are well described by spin waves in the ordered magnetic state for temperatures less than $T_N = 17$ K. The magnetic excitation spectrum consists of a 3.5 meV band of excitations with a gap of 2.2 meV. The first magnetic Bragg peak is at $Q = 1.06 \text{ \AA}^{-1}$. The large spin-quanta yields a significant magnetic cross-section in the ordered phase. No significant phonon scattering is observed for wave-vectors below 4 \AA^{-1} . The simple excitation spectrum and the energy scale of the excitations make CrCl_2 a reasonable candidate to compare performance of cold and thermal DGCS.

Measurements were performed using an identical sample at all four instruments. The sample consisted of approximately 5 g of CrCl_2 powder in a 1/4 in. diameter aluminum sample can. The sample was obtained commercially and loaded under a helium atmosphere. Identical software routines were used for processing the data. No time-independent background or empty can background subtraction is included in the data presented. No vanadium sensitivity correction has been applied to the data. A vanadium sensitivity correction is typically used with these instruments in order to account for variation in detector performance across the spectrometers' large detector arrays. The data have been normalized by the amount of beam current on the spallation target during the corresponding measurement. Data have been corrected for the energy dependent efficiency of the ^3He detector tubes. The data have been converted to the differential cross section by dividing by the energy bin width as well as being multiplied by the ratio of the incident and scattered wave-vector magnitudes ($\frac{K_i}{K_f}$). A detector mask has been applied to each measurement to remove the pixels at the ends of the ^3He detector tubes, as the end positions (approximately 5 cm at each end) of the LPSD used in these instruments have been found to be less sensitive to neutrons. We have also masked portions of the detector arrays which include any significant forward scattering due to beam divergence in the vicinity of the beam stop, and any detectors which were not operating properly.

The CNCS measurements were performed at $T = 5$ K. For the incident energies $E_i = 15$ meV and 7 meV, the instrument was operated in the intermediate mode with chopper speeds at 60, 60, 60, 240, and 240 Hz for choppers one through five, respectively. The measurements were performed during May 2012. We note the amount of charge accumulated on the spallation target in the captions of each dataset presented.

The HYSPEC measurements were performed at $T = 5$ K for $E_i = 7$ meV and 15 meV. The instrument was operated in a high flux mode with chopper speeds at 30, 60, 60, and 300 Hz for choppers T_0 , T1A, T1B, and Fermi, respectively. The center of the detector vessel was located with the detector bank

oriented so that the scattering angles of -66° to -6° were accessible, and one set acquired with the detector array straddling the incident beam making scattering angles -30° to 30° accessible. The measurements were performed in September of 2013.

The SEQUOIA measurements were performed at $T = 6.2$ K with $E_i = 15.1$ meV and $E_f = 7$ meV. For the 15/7 meV configuration, the T_0 chopper was set to a speed of 30 Hz while the 100 meV Fermi chopper was operated at 180/120 Hz. The measurements were performed in August of 2012.

The ARCS measurements were performed at $T = 5$ K with $E_i = 15$ meV. The T_0 chopper was set to 90 Hz while the 100 meV Fermi chopper was operated at 180 Hz. The measurements were performed in March of 2012

A. $E_i = 7$ meV

The three spectra acquired with $E_i = 7$ meV are shown in Fig. 9. All three measurements observe a band of magnetic excitations between approximately 2 and 6 meV energy transfer. The larger scattering angle coverage for CNCS is immediately observed as a larger range of measured wave-vector transfers. The CNCS and HYSPEC measurements are plotted on the same intensity scale. There are differences in both neutron flux, energy resolution and wave-vector resolution in these spectra. The SEQUOIA data have an extra elastic line at approximately 5.5 meV energy transfer. This is an extra opening in the T_0 chopper and Fermi chopper combination. These extra openings are well understood and are routinely used at SEQUOIA for implementing rep-rate multiplication where monochromatic measurements using multiple incident energies are measured simultaneously.⁴²

Figure 10 shows a constant wave-vector scan through the magnetic spectra for $1.0 < Q < 1.1 \text{ \AA}^{-1}$ for $E_i = 7$ meV. All three instruments have suitable flux for measurements at this incident energy. The measured scattering intensity is less at SEQUOIA than at CNCS and HYSPEC. HYSPEC has the greatest scattering intensity in this comparison albeit with the largest energy resolution. Figure 11 shows the measured elastic scattering obtained by integrating between $-0.5 < \hbar\omega < 0.5$ meV for the data shown in Fig. 9 as a function of wave-vector transfer for the three instruments. The CNCS measurement extends to larger wave-vectors due to the greater scattering angle coverage. The peaks at $Q \approx 1.06$ and 1.14 \AA^{-1} were fit to two Gaussians with the same width for the three measurements. The peak area for the HYSPEC measurement is roughly twice that of CNCS and 13 times that of SEQUOIA, although the background is approximately 3 times that of CNCS and 12 times that of the SEQUOIA measurement. The FWHM of the Gaussian peaks are 0.051(3), 0.038(3), and 0.029(2) for CNCS, HYSPEC, and SEQUOIA, respectively. The peak positions in wave-vector transfer are represented accurately for each instrument. The instrumental differences in wave-vector resolution, ranges of detector coverage, and flux as well as sample characteristics should be taken into consideration when choosing an instrument for a particular experiment in this range of incident energy.

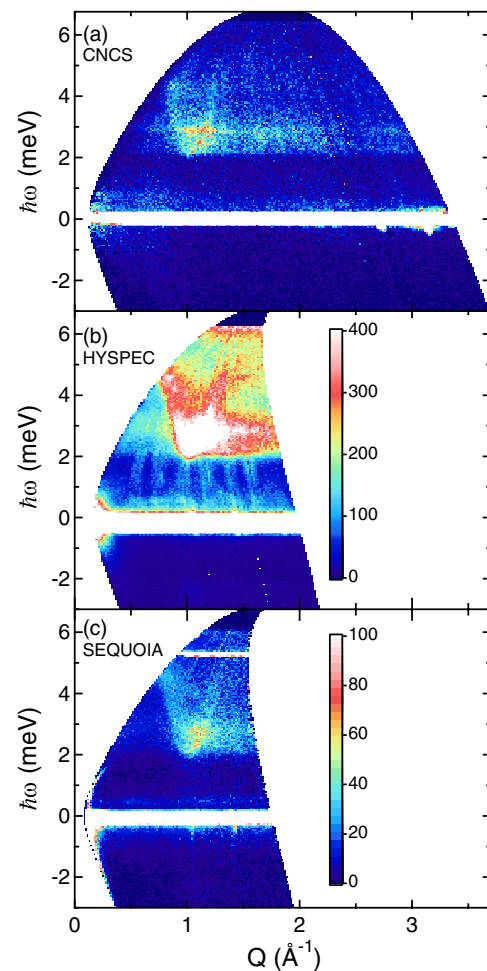


FIG. 9. Low-temperature spectra of CrCl_2 measured using the (a) CNCS, (b) HYSPEC, and (c) SEQUOIA spectrometers. Instrumental configurations are described in the text. Data have been reduced from time-of-flight measurements in an identical manner as described in the text. Panels (a) and (b) are plotted on the same intensity scale. Panel (c) is plotted on a separate intensity scale. The data are plotted with an energy binning of 0.05 meV and a 0.015 \AA^{-1} wave-vector binning. The data in (a)/(b)/(c) were acquired for 2/24.5/12 C of proton charge on the spallation target, respectively.

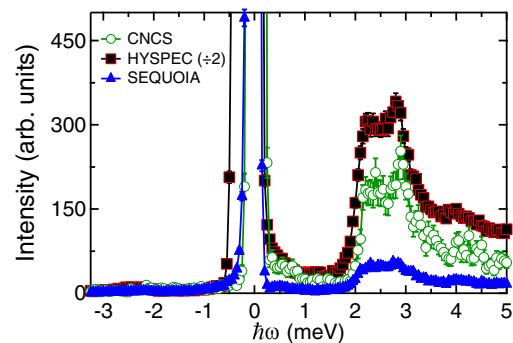


FIG. 10. Scattered neutron intensity as a function of energy transfer as measured CrCl_2 at $T \approx 5$ K using CNCS, HYSPEC, and SEQUOIA. Data correspond to integrating between $1.0 < Q < 1.1 \text{ \AA}^{-1}$ for the data shown in Fig. 9. Data were acquired for 2/24.5/12 C of proton charge on the spallation target for the CNCS/HYSPEC/SEQUOIA instruments, respectively. The HYSPEC data have been divided by a factor of 2 to place it on the same intensity scale as the other data shown.

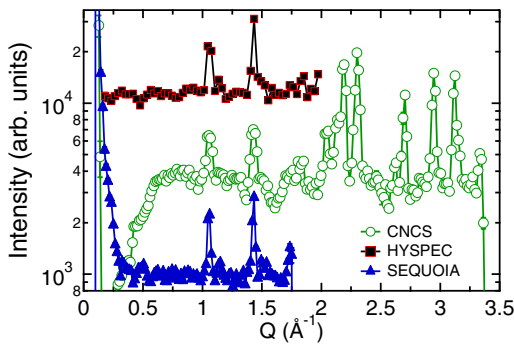


FIG. 11. Scattered neutron intensity as a function of wave-vector transfer as measured for CrCl_2 at $T \approx 5$ K using CNCS, HYSPEC, and SEQUOIA. Data correspond to integrating between $-0.5 < \hbar\omega < 0.5$ meV for the data shown in Fig. 9. Data were acquired for 2/24.5/12 C of proton charge on the spallation target for the CNCS/HYSPEC/SEQUOIA instruments, respectively.

Figure 12 shows the elastic scattering from these measurements at larger wave-vector transfer. This region of wave-vector transfer does not have any magnetic or nuclear Bragg peaks. The solid lines in Fig. 12 are Gaussian fits between -1 and 1 meV energy transfer. HYSPEC has a slightly asymmetric elastic lineshape. The ratios of the fitted areas under the Gaussian peaks are 1.00:0.27:0.09 for HYSPEC:CNCS:SEQUOIA. One measure of the signal to noise for these data is the ratio of the fitted Gaussian peak area to the average background signal between 0.5 and 1.5 meV energy transfer. These values are 66.9, 82.4, and 102 for HYSPEC, CNCS, and SEQUOIA, respectively. Again, we note that no vanadium sensitivity correction was applied to these measurements. Such corrections are able to account for variation in detector performance. Although HYSPEC has the largest area under the elastic peak position, CNCS has improved signal to noise and SEQUOIA has an even greater signal to noise with one tenth the total neutrons on sample. The fitted FWHM values are 0.17, 0.27, and 0.16 meV for CNCS, HYSPEC, and SEQUOIA. When choosing between these instruments one must consider that for $E_i = 7$ meV HYSPEC has a flux advantage over CNCS and SEQUOIA with a

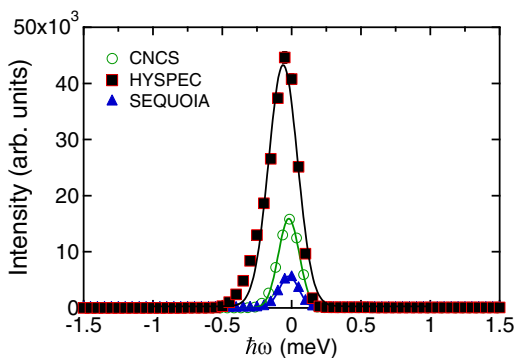


FIG. 12. Scattered neutron intensity as a function of energy transfer as measured for CrCl_2 at $T \approx 5$ K using CNCS, HYSPEC, and SEQUOIA. Data correspond to integrating between $1.5 < Q < 1.7$ \AA^{-1} for the data shown in Fig. 9. Data were acquired for 2/24.5/12 C of proton charge on the spallation target for the CNCS/HYSPEC/SEQUOIA instruments, respectively. Solid lines correspond to Gaussian fits between -1 and 1 meV energy transfer.

reduced energy resolution and detector coverage. At this incident energy, CNCS has a flux advantage over SEQUOIA, but the two instruments are well matched in resolution. Nevertheless, for an experiment one must consider whether there are features that must be examined at lower energy transfers or large momentum transfers where CNCS likely has the advantage, or larger energy transfers where SEQUOIA likely has the advantage.

B. $E_i = 15$ meV

The four spectra acquired with $E_i = 15$ meV are shown in Fig. 13. Again, one sees a similar band of magnetic excitations between approximately 2 and 6 meV energy transfer. Both ARCS and CNCS are able to measure at larger wave-vectors due to their larger scattering angle coverage. All four measurements are plotted on the same intensity scale (same scale as used in Figs. 9(a) and 9(b)). The SEQUOIA data have

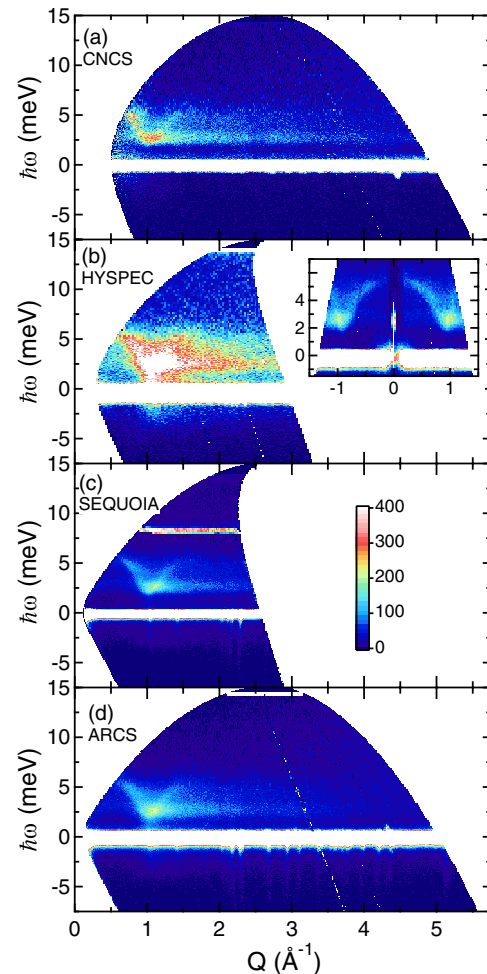


FIG. 13. Low-temperature spectra of CrCl_2 measured using the (a) CNCS, (b) HYSPEC, (c) SEQUOIA, and (d) ARCS spectrometers with $E_i = 15$ meV. Instrumental configurations are described in the text. A second spectrum was acquired at HYSPEC with detector coverage from -30° to 30° scattering angle (inset). Data have been reduced from time-of-flight measurements in an identical manner as described in the text. All panels are plotted on the same intensity scale. The data are plotted with an energy binning of 0.1 meV and a 0.015 \AA^{-1} wave-vector binning. The data in (a)/(b)/(c)/(d) were acquired for 2/2.3/12/5.4 C of proton charge on the spallation target, respectively.

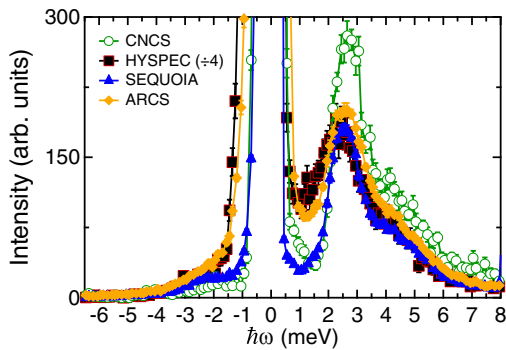


FIG. 14. Intensity as a function of energy transfer as measured for CrCl_2 at $T \approx 5$ K using CNCS, HYSPEC, ARCS, and SEQUOIA. Data correspond to integrating between $1.0 < Q < 1.1 \text{ \AA}^{-1}$ for the data shown in Fig. 13. Data were acquired for 2/2.3/12/5.4 C of proton charge on the spallation target for the CNCS/HYSPEC/SEQUOIA/ARCS instruments, respectively, with $E_i = 15$ meV. The HYSPEC data have been divided by a factor of 4 to place it on the same intensity scale as the other data shown.

a sharp line at approximately 8.4 meV energy transfer. This line arises from the prompt pulse of neutrons from the next frame and limits the size of the measurement window. One can see for CrCl_2 this incident energy is ideal, but careful consideration of the location of additional prompt pulses should be made for all of the spectrometers when planning the experiment. Note this is different from the sharp line seen in the $E_i = 7$ meV measurement, caused by extra opening in the T_0 and Fermi chopper combination. Both CNCS and HYSPEC are well suited for these incident energies with CNCS having finer energy resolution and HYSPEC having greater neutron flux and the potential to measure at very low scattering angles.

Figure 14 shows a constant wave-vector scan through the magnetic spectra for $1.0 < Q < 1.1 \text{ \AA}^{-1}$. SEQUOIA and CNCS have comparable energy resolution in this configuration, and HYSPEC has the greatest flux but with comparable energy resolution to the ARCS instrument. Although the error bars on the CNCS data are larger than the other measurements, we note that it was counted for the least amount of charge on the spallation target.

Figure 15 shows the measured elastic scattering as a function of wave-vector transfer for the four instruments. The CNCS and ARCS measurements extend to larger wave-vectors due to the greater scattering angle coverage. The inset shows the data plotted over a narrow range of wave-vector transfer. The ARCS and CNCS wave-vector resolution is comparable at this incident energy and the SEQUOIA resolution is better than all of the other instruments. The inset shows that the measured scattering intensity and signal to noise ratio is comparable for these three measurements. We fit the data between 1.95 and 2.5 \AA^{-1} to four Gaussian peaks with one width. The fitted FWHM values are $0.065(1)$, $0.047(1)$, $0.0383(7)$, and $0.0488(8) \text{ \AA}^{-1}$ for the CNCS, HYSPEC, SEQUOIA, and ARCS instruments, respectively. Just as in the $E_i = 7$ meV measurement SEQUOIA has the best wave-vector resolution. The total integrated area of these four peaks allows one to compare the measured scattering intensity. The areas of these four fitted peaks are $760(30)$, $2530(70)$, $510(25)$, and $640(30)$ for CNCS, HYSPEC, SEQUOIA, and ARCS, respectively.

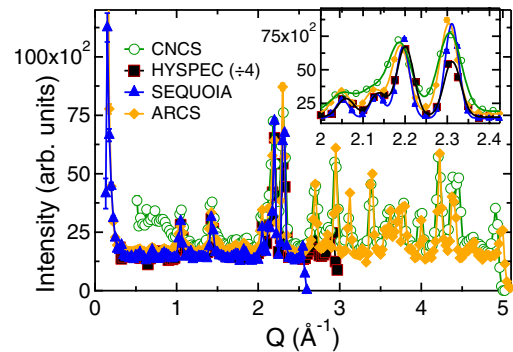


FIG. 15. Intensity as a function of wave-vector transfer as measured for CrCl_2 at $T \approx 5$ K using CNCS, HYSPEC, SEQUOIA, and ARCS. Data correspond to integrating between $-1.25 < \hbar\omega < 1.25$ meV for the data shown in Fig. 13. Data were acquired for 2/2.3/12/5.4 C of proton charge on the spallation target for the CNCS/HYSPEC/SEQUOIA/ARCS instruments, respectively, with $E_i = 15$ meV. The inset is plotted over a narrow range of wave-vector transfer to illustrate differences in the wave-vector resolution. The solid lines in the inset are fits to four Gaussian peaks with the same width as described in the text. The HYSPEC data have been divided by a factor of 4 to place it on the same intensity scale as the other data shown.

Figure 16 shows the elastic scattering from these measurements at larger wave-vector transfer. The solid lines in Fig. 16 are Gaussian fits between -1.5 and 1.5 meV energy transfer. ARCS and HYSPEC have a slightly asymmetric elastic lineshape. The fitted areas are all within a factor of 3 of one another for this measurement: $5010(20)$, $13000(2000)$, $3450(30)$, and $4270(30)$ for CNCS, HYSPEC, SEQUOIA, and ARCS, respectively. The fitted FWHM values are $0.425(9)$, $0.69(3)$, $0.321(9)$, and $0.56(1)$ meV for the CNCS, HYSPEC, SEQUOIA, and ARCS measurements. ARCS begins to have a reasonable flux for incident energies between $E_i = 7$ and 15 meV. For larger incident energies, the divergence and loss of flux at CNCS makes it less efficient.

A single measurement at HYSPEC was also examined with the detector tank straddling the incident beam. In this configuration the center of the detector bank is set to zero scattering angle. To reduce the divergence of the incident beam, a 20 minute Soller collimator was placed prior to

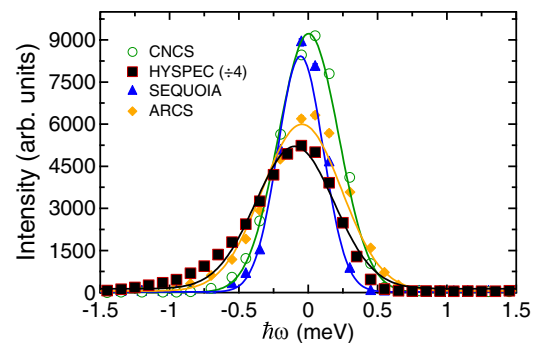


FIG. 16. Intensity as a function of energy transfer as measured for CrCl_2 at $T \approx 5$ K using CNCS, HYSPEC, SEQUOIA, and ARCS. Data correspond to integrating between $1.5 < Q < 1.7 \text{ \AA}^{-1}$ for the data shown in Fig. 13 with $E_i = 15$ meV. Data were acquired for 2/2.3/12/5.4 C of proton charge on the spallation target for the CNCS/HYSPEC/SEQUOIA/ARCS instruments, respectively. Solid lines correspond to Gaussian fits between -1.5 and 1.5 meV energy transfer.

the sample. In addition a 1 cm wide beam stop was placed approximately 30 cm downstream of the sample position. The incident beam collimation decreased the scattering intensity by a factor of approximately 3.4 for the 15 meV incident energy neutrons used. The inset to Fig. 13(b) shows the scattering intensity measured using this mode of the instrument. This mode works well down to approximately 3° – 4° scattering angle. Below this angle, there is the potential for spurious scattering or unreliable measurements of the scattering intensity. Using incident beam collimation may allow one to use this mode of operation, and average over both sides of the detector in order to improve the signal to noise ratio compared to keeping the entire detector tank to the left or the right of the incident neutron beam. When operating with the detector tank completely to one side of the beam, HYSPEC is able to measure scattering angles down to between 4° and 6° .

V. CONCLUSIONS

The measurements presented illustrate how the four direct geometry chopper spectrometers at the SNS compare to one another. We again note that these instruments are able to work with different chopper frequencies in order to tune the resolution and flux for a particular incident energy. We only present data from one experiment configuration for comparison.

The comparison of the incident neutron spectra available at these instruments for different operating configurations should also serve to help in matching the DGCS for the particular measurement being pursued. There are many factors to consider when choosing one of these instruments for an inelastic neutron scattering measurement. As in other neutron scattering instrumentation, there is always the balance of flux and resolution. That is, improving wave-vector and/or energy resolution comes at the cost of neutrons being counted in the detector. Knowing the energy and wave-vector bounds of the spectra to be measured helps to narrow down the choice of instrument. Alternatively, one may choose to use a particular instrument because of the ability to work over a large range of incident energies in order to determine the bounds of a spectrum. There are also beam time economic factors such as subscription rates which may affect the choice of instrument. When comparing the total number of days requested during a user proposal call against the number of days available for the instrument, the DGCS suite is consistently over-subscribed, with a typical factor ranging from 2 to 4.

There are upgrade paths for each of these four spectrometers. Both CNCS and SEQUOIA are planning to build out their entire detector coverage in the next five years. This will increase the number detectors at CNCS and SEQUOIA to 3 and 1.67 times their current number, respectively. CNCS is also scheduled to have additional neutron guide options purchased. These guides would be placed immediately before the sample to tailor a focused beam on samples of different sizes in order to maximize the neutron flux on the sample. Moving chopper positions is also being considered for CNCS. The chopper positions would be moved in order to use rep-rate multiplication techniques over a large range of incident ener-

gies. The polarization analysis packages at HYSPEC are being manufactured and scheduled testing will begin in 2014. Polarization techniques are also being considered for use at CNCS. Both ARCS and SEQUOIA can accommodate an additional T_0 or other pulse shaping chopper immediately after the primary T_0 chopper. This hardware is currently being considered.

There are several beam ports still available at the SNS. Considering the energy vs. wave-vector phase diagram of Fig. 8, there are at least two additional types of spectrometers which could find additional demand at the SNS. One would be a machine that concentrates on the first Brillouin zone with good energy and wave-vector resolution up to energy transfers between 2 and 200 meV. This machine would require operating at scattering angles as low as 0.5° . Another type of instrument being considered would be a spectrometer that has good detector coverage from approximately 3° up to approximately 150° or 160° scattering angle with an energy resolution between 1% and 3%. The PHAROS spectrometer at the Lujan neutron scattering center has a range of scattering angles between -10° and 145° with an energy resolution between 1% and 4%.⁸ A PHAROS like spectrometer at the SNS would be capable of higher resolution phonon measurements than the ARCS instrument albeit with a reduced neutron flux. A direct geometry chopper spectrometer instrument would likely be considered for several of the beam ports at the currently proposed second target station of the SNS. This target station will be a short pulse source optimized for longer wavelength neutrons with a lower repetition rate, most likely 10 Hz. A high-resolution cold neutron chopper spectrometer would be an excellent fit for this type of source. Thermal and epithermal direct geometry spectrometers would also be appropriate for such a source, and could make use of rep-rate multiplication techniques to improve efficiency of measurements.

ACKNOWLEDGMENTS

The research at Oak Ridge National Laboratory's Spallation Neutron Source was sponsored by the Scientific User Facilities Division, Office of Basic Energy Sciences, U.S. Department of Energy. D. L. Abernathy thanks J. M. Carpenter for suggestions regarding the modified Ikeda-Carpenter function described in the text.

¹B. N. Brockhouse and A. T. Stewart, *Rev. Mod. Phys.* **30**, 236 (1958).

²G. Shirane, S. M. Shapiro, and J. M. Tranquada, *Neutron Scattering with a Triple Axis Spectrometer* (Cambridge University Press, 2002).

³T. Heitmann and W. Montfrooij, *Practical Neutron Scattering at a Steady State Source* (Mizzou Media, Columbia, MO, 2012).

⁴K. Sköld and D. L. Price, *Methods of Experimental Physics*; v.23: *Neutron Scattering* (Academic Press Inc., Orlando, FL, 1986).

⁵C. Windsor, *Pulsed Neutron Scattering* (Taylor & Francis, London, UK, 1981).

⁶R. E. Lechner, in *Proceedings of the Workshop on Neutron Scattering Instrumentation for SNQ, Maria Laach 1984*, edited by R. Scherm and H. Stiller (KFA-Jülich, October 1984), pp. 202–220.

⁷C.-K. Loong, S. Ikeda, and J. M. Carpenter, *Nucl. Instrum. Methods Phys. Res. A* **260**, 381 (1987).

⁸R. J. McQueeney and R. A. Robinson, *Neutron News* **14**, 36 (2003).

⁹R. S. Eccleston, R. Osborn, and B. G. B. Kitchener, RAL Report No. RAL-94117, 1994.

- ¹⁰A. D. Taylor, R. C. Ward, W. G. Williams, Y. Endoh, and N. Watanabe, in *Proceedings of the 9th Meeting of the International Collaboration on Advanced Neutron Sources (ICANS IX)*, 1987.
- ¹¹T. G. Perring, A. D. Taylor, R. Osborn, D. Mck Paul, A. T. Boothroyd, and G. Aepli, in *Proceedings of the 12th Meeting of the International Collaboration on Advanced Neutron Sources (ICANS XII)*, 1993, RAL Report 94-025 (Rutherford Appleton Laboratory, Didcot, UK, 1994), p. I-60.
- ¹²R. I. Bewley, R. S. Eccleston, K. A. McEwen, S. M. Hayden, M. T. Dove, S. M. Bennington, J. R. Treadgold, and R. L. S. Coleman, *Physica B* **385–386**, 1029–1031 (2006).
- ¹³R. I. Bewley, T. Guidi, and S. M. Bennington, *Notiziario Neutroni Luce Sincrotrone* **14**, 22–27 (2009).
- ¹⁴R. I. Bewley, J. W. Taylor, and S. M. Bennington, *Nucl. Instrum. Methods Phys. Res. A* **637**, 128–134 (2011).
- ¹⁵R. I. Bewley, J. W. Taylor, and S. M. Bennington, *Notiziario Neutroni Luce Sincrotrone* **16**(2), 4–13 (2011).
- ¹⁶R. Kajimoto, T. Yokoo, K. Nakajima, M. Nakamura, K. Soyama, T. Ino, S. Shamoto, M. Fujita, K. Ohoyama, H. Hiraka, K. Yamada, and M. Arai, *J. Neutron Res.* **15**, 5–12 (2007).
- ¹⁷S. Itoh, T. Yokoo, S. Satoh, S.-i. Yano, D. Kawana, J. Suzuki, and T. J. Sato, *Nucl. Instrum. Methods Phys. Res. A* **631**, 90 (2011).
- ¹⁸K. Nakajima, S. Ohira-Kawamura, T. Kikuchi *et al.*, *J. Phys. Soc. Jpn.* **80**, SB028 (2011).
- ¹⁹G. Ehlers, A. A. Podlesnyak, J. L. Niedziela, E. B. Iverson, and P. E. Sokol, *Rev. Sci. Instrum.* **82**, 085108 (2011).
- ²⁰G. E. Granroth, A. I. Kolesnikov, T. E. Sherline, J. P. Clancy, K. A. Ross, J. P. C. Ruff, B. D. Gaulin, and S. E. Nagler, *J. Phys.: Conf. Ser.* **251**, 012058 (2010).
- ²¹D. L. Abernathy, M. B. Stone, M. J. Loguillo, M. S. Lucas, O. Delaire, X. Tang, J. Y. Y. Lin, and B. Fultz, *Rev. Sci. Instrum.* **83**, 015114 (2012).
- ²²D. L. Abernathy, “Optimizing Fermi-chopper spectrometers for the Spallation Neutron Source,” *Appl. Phys. A: Mater. Sci. Process.* **74**, s1595–s1597 (2002).
- ²³G. E. Granroth and D. L. Abernathy, in *Proceedings of ICANS-XVI* (Forschungszentrum Jülich GmbH, Jülich, Germany, 2003), p. 289.
- ²⁴S. M. Shapiro, I. Zaliznyak, L. Passell, and V. Ghosh, in *Proceedings of ICANS-XVI* (Forschungszentrum Jülich GmbH, Jülich, Germany, 2003), p. 191.
- ²⁵Publication lists for the instruments are available at <http://neutrons.ornl.gov/media/pubs/> and at each instruments web page as listed at <http://neutrons.ornl.gov/instruments/>.
- ²⁶G. J. Russell, E. J. Pitcher, G. Muhrer, F. Mezei, and P. D. Ferguson, “Overview of Spallation Neutron Source Physics,” *Fundamental Physics with Pulsed Neutron Beams* (World Scientific, 2000), p. 19.
- ²⁷SNS Parameters List, SNS Technical Document SNS 10000000-PL0001-R13, 2005.
- ²⁸E. B. Iverson, P. D. Ferguson, F. X. Gallmeier, and I. I. Popova, “Detailed SNS neutronics calculations for scattering instrument design: SCT configuration,” Spallation Neutron Source Report No. SNS 110040300-DA0001-R00, 2002.
- ²⁹R. Riedel, R. Cooper, L. Funk, and L. Clonts, *Nucl. Instrum. Methods Phys. Res. A* **664**(1), 366 (2012).
- ³⁰H. Nojiri, S. Yoshii, M. Yasui, K. Okada, M. Matsuda, J.-S. Jung, T. Kimura, L. Santodonato, G. E. Granroth, K. A. Ross, J. P. Carlo, and B. D. Gaulin, *Phys. Rev. Lett.* **106**, 237202 (2011).
- ³¹See <http://dx.doi.org/10.5286/Software/Mantid3.0> for The Mantid Project.
- ³²F. Weber, S. Rosenkranz, L. Pintschovius, J.-P. Castellán, R. Osborn, W. Reichardt, R. Heid, K.-P. Bohnen, E. A. Goremychkin, and D. L. Abernathy, *Phys. Rev. Lett.* **109**, 057001 (2012).
- ³³C. Y. Jiang, X. Tong, D. R. Brown, H. Culbertson, M. K. Graves-Brook, M. E. Hagen, B. Kadron, W. T. Lee, J. L. Robertson, and B. Winn, “Spin exchange optical pumping based polarized ³He filling station for the hybrid spectrometer at the Spallation Neutron Source,” *Rev. Sci. Instrum.* **84**, 065108 (2013).
- ³⁴G. E. Granroth, D. H. Vandergriff, and S. E. Nagler, *Phys. B.: Condens. Matter* **385–386**, 1104–1106 (2006).
- ³⁵S. Ikeda and J. M. Carpenter, *Nucl. Instrum. Methods Phys. Res. A* **239**, 536 (1985).
- ³⁶See supplementary material at <http://dx.doi.org/10.1063/1.4870050> for additional figures illustrating beam monitor measurements as a function of incident energy.
- ³⁷J. W. Cable, M. K. Wilkinson, and E. O. Wollan, *Phys. Rev.* **118**, 950 (1960).
- ³⁸J. W. Tracy, N. W. Gregory, E. C. Linafelter, J. D. Dunitz, H.-C. Mez, R. E. Rundle, C. Scherlinger, H. L. Yakel, Jr., and M. K. Wilkinson, *Acta Cryst.* **14**, 927 (1961).
- ³⁹H. R. Oswald, *Helv. Chim. Acta* **44**, 1049 (1961).
- ⁴⁰A. Hermann, B. Vest, and P. Schwerdtfeger, *Phys. Rev.* **74**, 224402 (2006).
- ⁴¹M. B. Stone, G. Ehlers, and G. E. Granroth, *Phys. Rev. B* **88**, 104413 (2013).
- ⁴²J. P. Carlo, J. P. Clancy, K. Fritsch, C. A. Marjerrison, G. E. Granroth, J. E. Greedan, H. A. Dabrowska, and B. D. Gaulin, *Phys. Rev. B* **88**, 024418 (2013).